

## Article

# Synthesis of C/SiC Mixtures for Composite Anodes of Lithium-Ion Power Sources

Anastasia M. Leonova <sup>1,\*</sup>, Oleg A. Bashirov <sup>1</sup>, Natalia M. Leonova <sup>1</sup>, Alexey S. Lebedev <sup>2</sup>,  
Alexey A. Trofimov <sup>1,3</sup> and Andrey V. Suzdaltsev <sup>1,3,\*</sup>

<sup>1</sup> Scientific Laboratory of the Electrochemical Devices and Materials, Ural Federal University, Mira St. 28, 620002 Yekaterinburg, Russia

<sup>2</sup> South Urals Research Center of Mineralogy and Geoecology UB RAS, Ilmen Reservation, 456317 Miass, Russia

<sup>3</sup> Scientific-Research Department of Electrolysis, Institute of High-Temperature Electrochemistry UB RAS, Akademicheskaya St. 20, 620137 Yekaterinburg, Russia

\* Correspondence: a.m.leonova@urfu.ru (A.M.L.); a.v.suzdaltsev@urfu.ru (A.V.S.)

**Abstract:** Nowadays, research aimed at the development of materials with increased energy density for lithium-ion batteries are carried out all over the world. Composite anode materials based on Si and C ultrafine particles are considered promising due to their high capacity. In this work, a new approach for carbothermal synthesis of C/SiC composite mixtures with SiC particles of fibrous morphology with a fiber diameter of 0.1–2.0  $\mu\text{m}$  is proposed. The synthesis was carried out on natural raw materials (quartz and graphite) without the use of complex equipment and an argon atmosphere. Using the proposed method, C/SiC mixture as well as pure SiC were synthesized and used to manufacture anode half-cells of lithium-ion batteries. The potential use of the resulting mixtures as anode material for lithium-ion battery was shown. Energy characteristics of the mixtures were determined. After 100 cycles, pure SiC reached a discharge capacity of 180 and 138  $\text{mAh g}^{-1}$  at a current of C/20 and C, respectively, and for the mixtures of (wt%) 29.5C–70.5 SiC and 50Si–14.5C–35.5SiC discharge capacity of 328 and 400  $\text{mAh g}^{-1}$  at a current of C/2 were achieved. The Coulombic efficiency of the samples during cycling was over 99%.

**Keywords:** lithium-ion battery; silicon carbide; electrodeposited silicon; composite material; anode material; Coulombic efficiency



**Citation:** Leonova, A.M.; Bashirov, O.A.; Leonova, N.M.; Lebedev, A.S.; Trofimov, A.A.; Suzdaltsev, A.V. Synthesis of C/SiC Mixtures for Composite Anodes of Lithium-Ion Power Sources. *Appl. Sci.* **2023**, *13*, 901. <https://doi.org/10.3390/app13020901>

Academic Editor: Gajnd P. Pandey

Received: 15 December 2022

Revised: 2 January 2023

Accepted: 6 January 2023

Published: 9 January 2023



**Copyright:** © 2023 by the authors. Licensee MDPI, Basel, Switzerland. This article is an open access article distributed under the terms and conditions of the Creative Commons Attribution (CC BY) license (<https://creativecommons.org/licenses/by/4.0/>).

## 1. Introduction

Graphite is traditionally used as an anode material of lithium-ion batteries (LIBS) due to its relatively low cost, low volume expansion (up to 10%), high electrical conductivity, charge rate. On the other hand, this material capacity (up to 372  $\text{mAh g}^{-1}$ ) [1–3] no longer meets the requirements of modern devices and machines for an increased energy density.

Promising anode materials with a higher specific capacity for LIBS are transition metal oxides [4–9], silicon [10–14], germanium [15–17], SiC [18,19], as well as various composite mixtures of the above materials with carbon [20–27]. Transition metal oxides seem to be cheap, easy to synthesize. They provide a relatively high capacity (theoretical up to 718  $\text{mAh g}^{-1}$  [4]; experimental up to 1150  $\text{mAh g}^{-1}$  [4]) and charge rate, but suffer from high volume expansion (about 96% [8]). Silicon also seems to be a suitable material that provides maximum capacity (theoretical up to 4200  $\text{mAh g}^{-1}$  [9–12], experimentally achieved—3900  $\text{mAh g}^{-1}$  [13]) and a sufficiently high charge rate, but drastic volume expansion (up to 300% [10–12]) still presents the biggest challenge to the realization of Si anodes. Germanium is a less accessible material with a lower capacity (theoretical, up to 1624  $\text{mAh g}^{-1}$ ; experimental, up to 1248  $\text{mAh g}^{-1}$  [16]) compared to silicon, but it provides advantages such as higher electronic conductivity. Moreover, the diffusion coefficient of lithium ions in germanium is 400 times higher than in silicon [17].

Silicon carbide is a perspective easily available anode material with high mechanical, chemical and thermal stability [18,19]. However, for lithiation, pure SiC must have a certain structure and size. Therefore, it is considered more as a matrix or substrate that allows to compensate the volume expansion of silicon. Nevertheless, several works have reported on the LIBs with SiC anode. In [28,29], a decrease in the thickness of SiC films or particles leads to an increase in their capacity from 300 to 1370 mAh g<sup>-1</sup> with a Coulombic efficiency of about 90%. This also explains the significant scatter of the SiC anode capacity in the available papers. Finally, recently a significant number of articles have been devoted to the development of LIBs with composite anode materials represented by silicon, graphite, SiC, SiO<sub>x</sub>, etc., including various sizes and structures: core-shell wires, tubes, needles, fibers, multilayer films of graphene and silicene [30–34]. Calculations showed improved electrochemical parameters of such structures during lithiation/delithiation [35]. Despite the advantages of such composite anodes, their relatively complex production should be noted. Often, single samples are presented in the existing works and nothing is reported about the large-scale production of the materials. At present, the carbothermal method is mainly used for the large-scale production of silicon carbide [36,37]. At the same time, many works are devoted to the metallothermic preparation of SiC [38,39], although these methods require further purification of carbide from intermediate synthesis products.

Previously, we showed the possibility of synthesizing ultrafine SiC fibers from cheap materials using carbothermal synthesis [40,41]. The feature of our method is the use of natural samples of pure quartz and graphite with a certain morphology and particle size. In this work, in addition to the obtaining of SiC, this approach was also used for obtaining of C/SiC mixtures suitable for use as composite anodes of lithium-ion power sources.

## 2. Materials and Methods

**Scheme of the synthesis:** The synthesis of SiC powder was carried out in a graphite crucible, which was placed in a protective alumina crucible. Mixture of SiO<sub>2</sub> and graphite powder with molar ratio of 1–3 was prepared by hand mixing in agate mortar and placed in a crucible. Graphite crucible was covered with graphite cap and buried under extra graphite layer. Synthesis was conducted at a temperature of 1600 °C for 5 h under CO atmosphere. In such reactor and conditions, the atmosphere maintained stable due to the oxidation of graphite powder [40,41]. The scheme for the synthesis of SiC-based mixtures with different compositions is shown in Figure 1. It was shown experimentally that mixtures with 40–95 wt% SiC and unreacted graphite are formed during synthesis depending on the given SiO<sub>2</sub>:C ratio, temperature and synthesis duration; the products may also contain traces of silicon and its nonstoichiometric oxides, which are removed by additional treatment in the HF solution. Therefore, the primary synthesis products are the C/SiC mixtures. The ratio of components in such mixtures can be controlled in order to obtain required mixture.

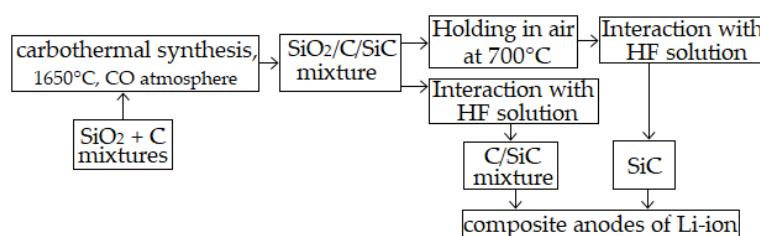


**Figure 1.** Process flow diagram for obtaining C/SiC mixtures for the manufacture of LIBs anodes.

In this work we synthesized a C/SiC mixture and pure SiC that were studied in the anode half-cell of LIBs. Along with these materials, a composite anode based on the resulting C/SiC mixture with the addition of electrodeposited silicon fibers from the KCl–K<sub>2</sub>SiF<sub>6</sub> melt was also tested [42].

**Analysis of the morphology and composition:** The chemical and phase composition of the reagents and products was determined by inductively coupled plasma atomic emission

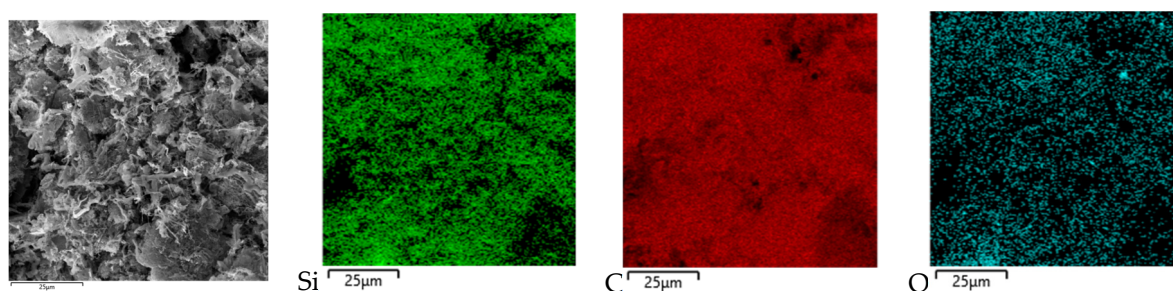
spectroscopy (AES-ICP) using iCAP 6300 Duo Spectrometer (Thermo Scientific, Waltham, MA, USA), X-ray phase analysis (XRD) using Rigaku D/MAX-2200VL/PC diffractometer (Rigaku, Tokyo, Japan) and Raman spectroscopy using U1000 Raman spectrometer (Renishaw, New Mills, UK). The morphology and elemental composition of the obtained samples were studied using a Tescan Vega 4 (Tescan, Brno–Kohoutovice, Czech Republic) scanning electron microscope with Xplore 30 EDS detector (Oxford, UK).

**Electrochemical performance:** Electrochemical performance of SiC, C/SiC and Si/C/SiC anodes were investigated in a 3-electrode half-cell. The obtained compositions were mixed with 10 wt% polyvinylidene fluoride dissolved in N-methyl-2-pyrrolidone without any other additives. LIBs anode half-cell fabrication was performed in an argon-filled glove box ( $O_2$ ,  $H_2O < 0.1$  ppm). Stainless steel mesh with the applied composite anode material was used as the working electrode and two separate lithium strips as the counter and reference electrodes. All electrodes were divided by 2 layers of polypropylene separator and tightly placed in the cell. The cell was filled with 1 mL of electrolyte—1 M  $LiPF_6$  in a mixture of ethylene carbonate/dimethyl carbonate/diethyl carbonate (1:1:1 by volume). Electrochemical measurements and cycling experiments were performed using a Zive-SP2 potentiostat (WonATech, Seoul, Republic of Korea).

### 3. Results

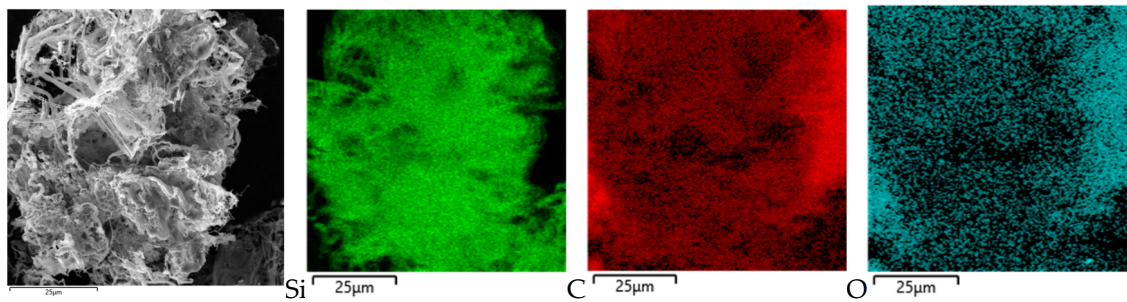
#### 3.1. Samples Characterization

**C/SiC mixtures:** Figure 2 shows a SEM-image of a C/SiC mixture and maps of elemental distribution after carbothermal synthesis and treatment in HF solution. The resulting mixture is represented by particles with a size of about 20–40 microns (graphite) and smaller fibers (SiC). According to X-ray microanalysis, the content of the elements was (wt%) silicon 47.5–51.3; carbon 47.7–51.7; oxygen—up to 1.6. The presence of oxygen could be due to both the insufficient treatment time of the mixture in the HF solution and the subsequent oxidation of the silicon or SiC presented in the mixture. According to ICP analysis, the resulting mixture contained 48.8–49.4 wt% silicon (the rest was carbon) and no more than 0.4 ppm of such impurities as Fe, Al, Ti and Ca. If we do not take into account the presence of oxygen, the ratio of components corresponds to a mixture of (wt%): 70.5SiC-29.5C.



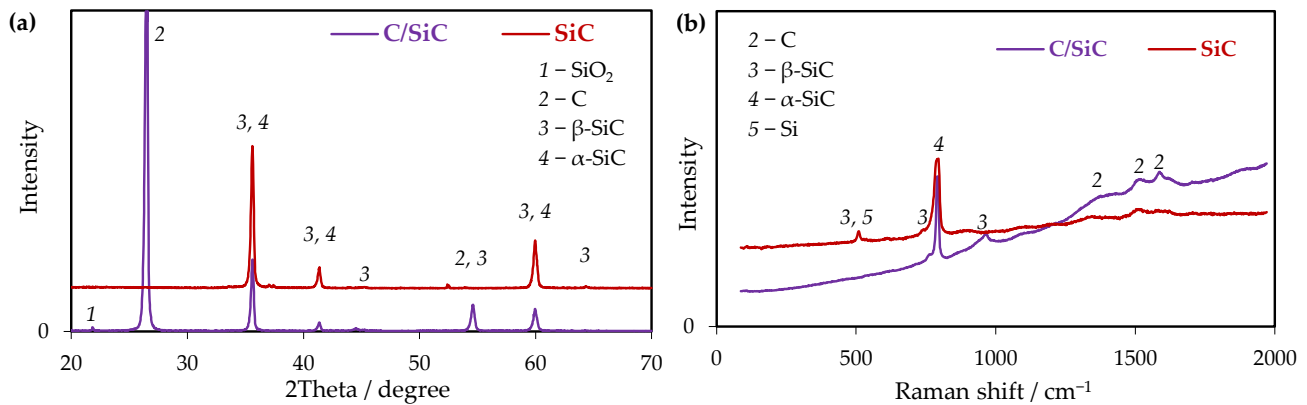
**Figure 2.** SEM-images and elements distribution in a C/SiC mixture after carbothermal synthesis and treatment in HF solution.

**SiC:** Figure 3 shows a SEM-image of a typical SiC agglomerate obtained after annealing of residual carbon from a C/SiC mixture. Its total size is about 50–60  $\mu m$ . It consists of fibers with a diameter of 0.1 to 2  $\mu m$ . The obtained morphology is similar to the previously obtained samples of ultrafine SiC [40] since the reagents and the synthesis procedure were reproduced almost completely. The distribution of elements in the resulting SiC are also shown. Uniform distribution of silicon, carbon and oxygen is observed for this sample. According to X-ray microanalysis, the average content of elements at different points of the sample was (wt%): 68–69 silicon, 29–30 carbon, up to 1.6 oxygen. This ratio is close to the SiC stoichiometric composition.



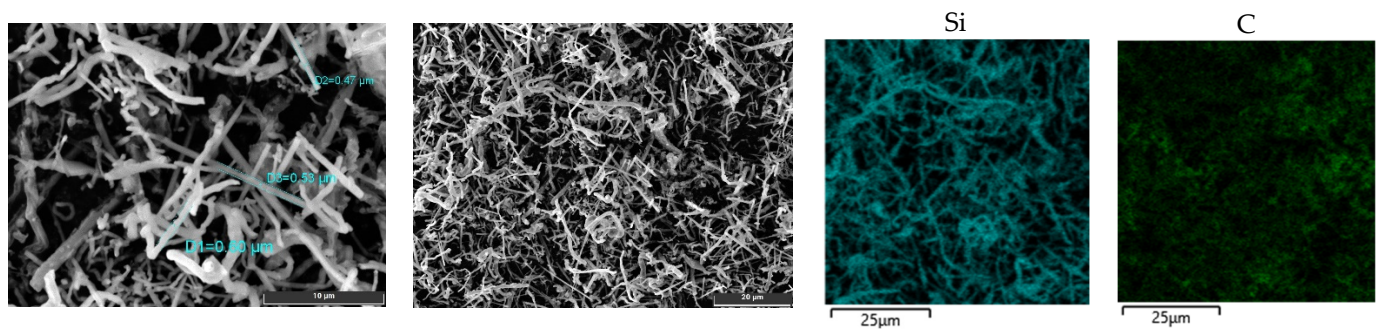
**Figure 3.** SEM-images and elements distribution in a SiC sample after carbothermal synthesis, oxidation of unreacted graphite, and treatment in HF solution.

Figure 4 shows the X-ray diffraction patterns and Raman spectra for C/SiC and SiC samples. For the C/SiC sample there are peaks of residual  $\text{SiO}_2$  ( $21\text{--}22^\circ$ ), carbon ( $26\text{--}27^\circ$ ), as well as peaks indicating presence of two carbide modifications ( $\alpha\text{-SiC}$ ,  $\beta\text{-SiC}$ ) in sample ( $35\text{--}36^\circ$ ,  $41.5^\circ$ ,  $44.5^\circ$ ,  $55^\circ$  and  $60^\circ$ ). For the SiC sample, there are no peaks of C and  $\text{SiO}_2$ ; only additional signals of the  $\beta\text{-SiC}$  phase appear at  $64.5^\circ$ . A similar picture is also observed in Raman spectra, in which responses of  $\alpha\text{-SiC}$  and  $\beta\text{-SiC}$  carbide modifications at  $770\text{--}793\text{ cm}^{-1}$  were fixed. In this case, for the SiC sample, there is also a response at  $502\text{ cm}^{-1}$  that can correspond to both residual silicon and the  $\beta\text{-SiC}$  modification [43]. Moreover, there are lines near  $1370$ ,  $1510$  and  $1585\text{ cm}^{-1}$  on both spectra, which indicate the C–C bonds. In this work, the structure of the used graphite powder was not studied in detail. However, based on the absence of pronounced peaks and intensity ratio of carbon lines, one can only note the presence of different carbon structures [44–47]. For the SiC sample, the intensities of these lines are less pronounced.

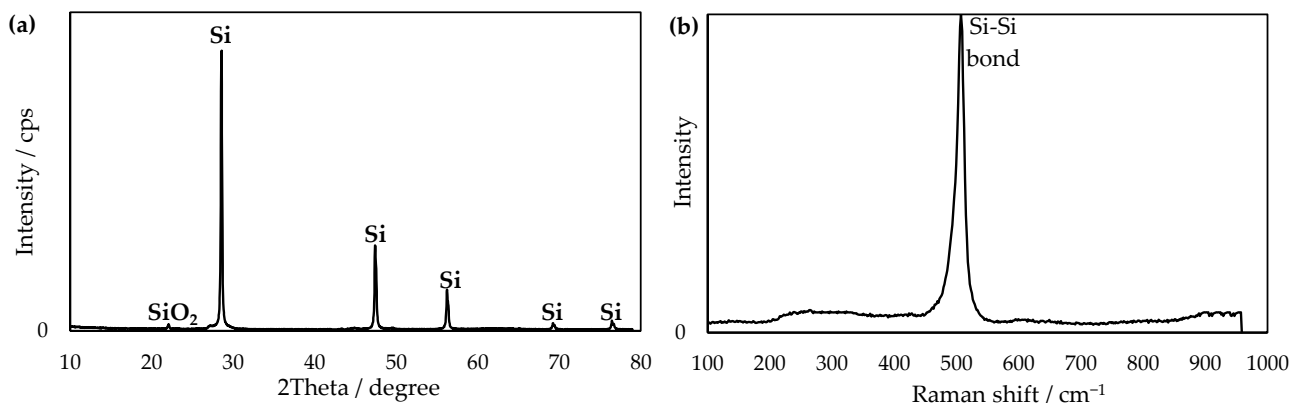


**Figure 4.** X-ray diffraction patterns (a) and Raman spectra (b) for the obtained C/SiC and SiC samples.

**Electrodeposited Si:** Figure 5 shows a SEM-image of silicon deposits obtained by electrolysis of the (wt%)  $98\text{KCl}\text{--}2\text{K}_2\text{SiF}_6$  melt at a temperature of  $780^\circ\text{C}$  and a cathode current density of  $25\text{ mA cm}^{-2}$ . A detailed procedure and parameters for silicon synthesis were provided earlier [42]. The resulting silicon deposits are arbitrarily shaped fibers with a diameter in the range of  $0.45\text{--}0.55\text{ }\mu\text{m}$  and a length of up to  $20\text{--}25\text{ }\mu\text{m}$ . According to X-ray microanalysis data, the oxygen content in the obtained silicon was from  $1.2$  to  $1.5\text{ wt}\%$  and other impurities did not exceed  $0.18\text{ ppm}$  (mainly iron and nickel). Figure 6 shows the X-ray diffraction pattern and the Raman spectra of silicon deposit. As can be seen, the sample is represented by polycrystalline silicon with  $\text{SiO}_2$  impurities. This is also indicated by the Raman spectra of the sample in which only the Si–Si bond at  $510\text{ cm}^{-1}$  was found [43].



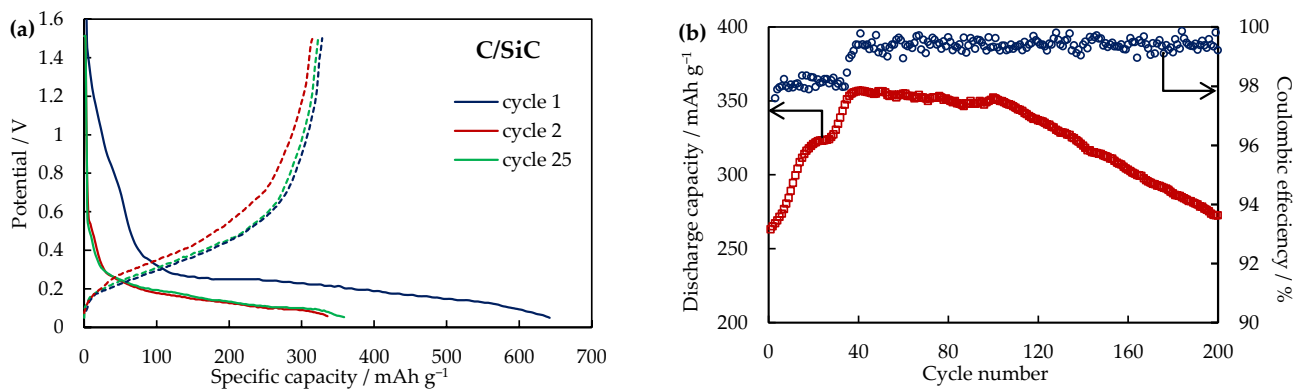
**Figure 5.** SEM-image and the elements distribution in a Si sample obtained by electrolysis of the (wt%) 98KCl-2K<sub>2</sub>SiF<sub>6</sub> melt at a temperature of 780 °C and a cathode current density of 25 mA cm<sup>-2</sup>.



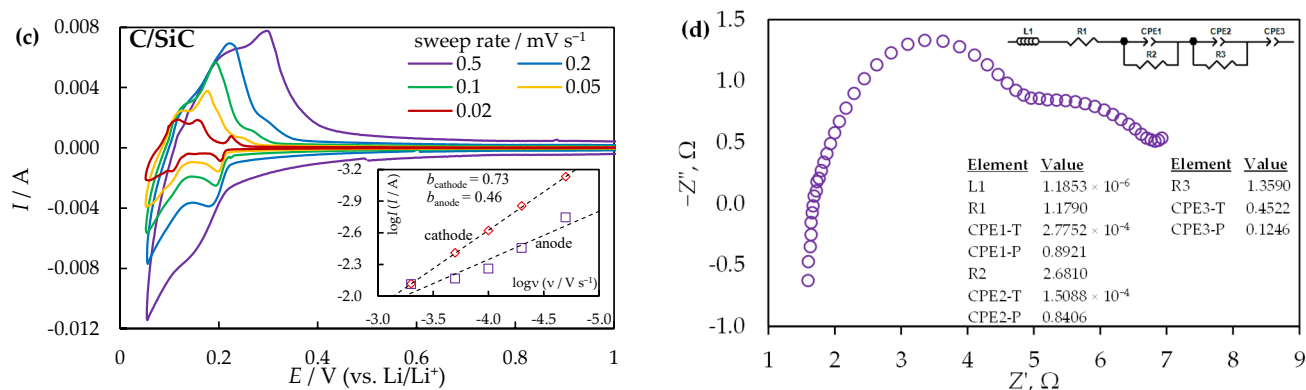
**Figure 6.** X-ray diffraction pattern (a) and the Raman spectra (b) of silicon deposit.

### 3.2. Electrochemical Performance of the Composite Anodes

C/SiC composite anode: Figure 7 shows the change in the C/SiC composite anode potential during lithiation/delithiation, as well as changes in the discharge capacity and Coulombic efficiency of the sample during cycling. When the C/SiC composite anode sample was initially charged with a current of 0.1 C (first cycle) its charging capacity was 658 and discharge capacity was 322 mAh g<sup>-1</sup> (Coulombic efficiency is 49%). Such capacity loss is usually attributed to a solid–electrolyte interface (SEI) layer formation. All subsequent cycling was carried out at a current of 0.5 C. In the second cycle, the discharge capacity was 308 mAh g<sup>-1</sup> (Coulombic efficiency is 92%), and after the 100th cycle the discharge capacity was 328 mAh g<sup>-1</sup> (see Figure 7c). During cycling, the Coulombic efficiency of the C/SiC anode reached 99% and remained at this level even after capacity began to fade.



**Figure 7.** Cont.



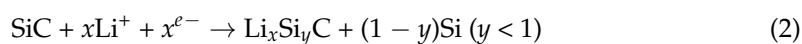
**Figure 7.** Cycling of C/SiC electrode: (a) potential change during lithiation (dashed line) and delithiation (solid line); (b) discharge capacity and Coulombic efficiency; (c) CVs at different scan rates and  $\log(I)$ – $\log(v)$  dependencies; (d) EIS data with equivalent circuit diagram.

Figure 7c shows current–voltage dependences (CVs) characterizing the kinetics of charge and discharge of a C/SiC composite anode material. It can be noted that the beginning of the charge occurs at an electrode potential negatively than 0.22 V relative to the potential of the lithium electrode. This behavior may be due to the interaction of lithium ions with the electrode material, which is accompanied by the chemical formation of compounds. In this case the presence of several peaks in the cathode region of the CVs indicates the occurrence of several lithiation reactions. At a potential of about 0.05 V a lithium reduction wave is formed. During discharge in the anodic region of the CVs in the potential range from 0.05 to 0.5 V there are corresponding discharge (oxidation) peaks of lithium. Moreover, the shift in the peak potentials of the lithium reduction and oxidation indicates that the processes is not electrochemically reversible. Obviously, the irreversibility may be due to the interaction of lithium with the anode material. Since the LIBs capacity includes the contribution of both diffusion and capacitance reactions the expression [48] is valid for the usual lithiation/delithiation process:

$$\log(I) = \log(a) + b \log(v) \quad (1)$$

where  $I$ —peak current, A;  $v$ —potential sweep rate, V s<sup>-1</sup>;  $a$  and  $b$ —constants. In our case, the calculated  $b$  value was of 0.73 (see Figure 7c), which indicates the pseudocapacitive behavior of the C/SiC anode material [48]. This may be associated with a slow chemical reaction of silicon carbide with lithium. Figure 7d shows the electrochemical impedance spectra (frequency range from 100,000 to 1 Hz) of the sample after the forming cycle. The EIS contains two arcs corresponding to the processes of charge transfer through the electrolyte layer and between the electrode and electrolyte [49–51]. The obtained data can be described by a typical for LIBs equivalent circuit. It has two RC circuits connected in series and a resistance (Figure 7e). Parameters changes in this scheme during cycling have not yet been studied.

**SiC anode:** The cycling results of the SiC electrode are shown in Figure 8. When the SiC electrode sample was initially charged at a current of  $C/20$  (first cycle) its charge capacity was only 78 and the discharge capacity was of 42 mA h g<sup>-1</sup> (Coulombic efficiency is 54%). During further cycling, the capacity gradually increased. After the 60 cycles at  $C/20$ , capacity increased up to 180 mA h g<sup>-1</sup>. This situation can be caused by gradual activation of the anode material accompanied by partial destruction of SiC and the formation of Li–C and Li–Si compounds [28,29] via the reactions:



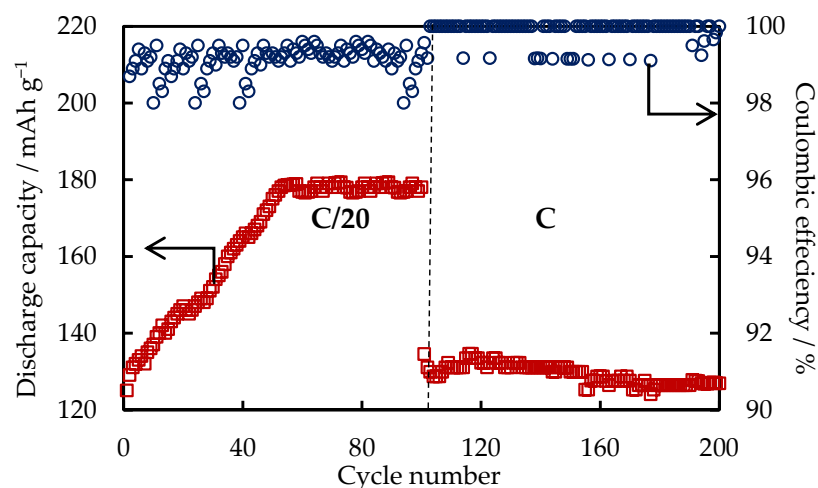


**Figure 8.** Changes in the discharge capacity and Coulombic efficiency of the SiC sample during cycling at a current of C/20 and C.

As a result, a gradual conversion of SiC to Si and C occurs [28,29]. In turn, reactions (1) and (2) also explain the reason for the onset of lithium discharge on anodes with SiC at a potential 0.22 V more positive than the lithium potential (see Figure 7b). With an increase in the charge current to C, the discharge capacity decreased, while its value was stable during 100 cycle and the Coulombic efficiency was more than 99.2%. Relatively low capacity can be explained by the presence of voids (see Figure 3) and a lack of the electrical contact between stiff SiC wires.

**Si/C/SiC anode:** Figure 9 shows the changes of the Si/SiC/C electrode potential during lithiation and delithiation as well as changes in its discharge capacity and Coulombic efficiency during cycling. A voltage plateau below 0.1 V (Figure 9a) indicates lithiation of graphite and silicon; delithiation occurs at 0.15–0.4 V. Similar results were obtained for lithiation of the silicon anode [52]. In the first cycle at a current of C/20, the discharge capacity was 225 mAh g<sup>-1</sup> and the initial Coulombic efficiency was 54%. Coulombic efficiency gradually increased during further cycling at a current of 0.5C and remained above 98% after 20 cycles (Figure 9b). The discharge capacity gradually increased up to 525 mAh g<sup>-1</sup> after 40 cycles. The higher capacity value can be explained by the silicon lithiation in the anode material and the additional increase during cycling can be explained by the gradual activation of the electrode, as in the case of the SiC anode (see Figure 8a). The subsequent decrease in the discharge capacity to 400 mAh g<sup>-1</sup> by the 100th cycle may be due to the contact loss of part of the anode material with the substrate due to the local expansion and cracking of silicon.

Figure 9c shows the CVs obtained at different scan rates for the Si/SiC/C electrode. There are clear redox peaks indicating the charge and discharge of the sample. In this case the calculated value of *b* was 0.63 (see Figure 9c). This indicates that the operation of the Si/C/SiC electrode mainly proceeds under lithium diffusion conditions. A distinctive feature of the obtained CVs is also the fact that the charge and discharge currents of the anode sample are observed in a wider potential range (0.8–0.1 and 0.1–1.4 V respectively), which is due to the higher bonding energy of lithium with silicon and a larger number of compounds in the Li–Si system [52–54].

Figure 9d shows the electrochemical impedance spectrum of the Si/C/SiC sample after the forming cycle. One can note the relatively high resistance R1 (7.7 Ω), which can result in a significant change in the parameters of two series-connected RC chains (R2, C2, R3 and W1) [49,50]. The decrease in R1 will be the subject of our further research.

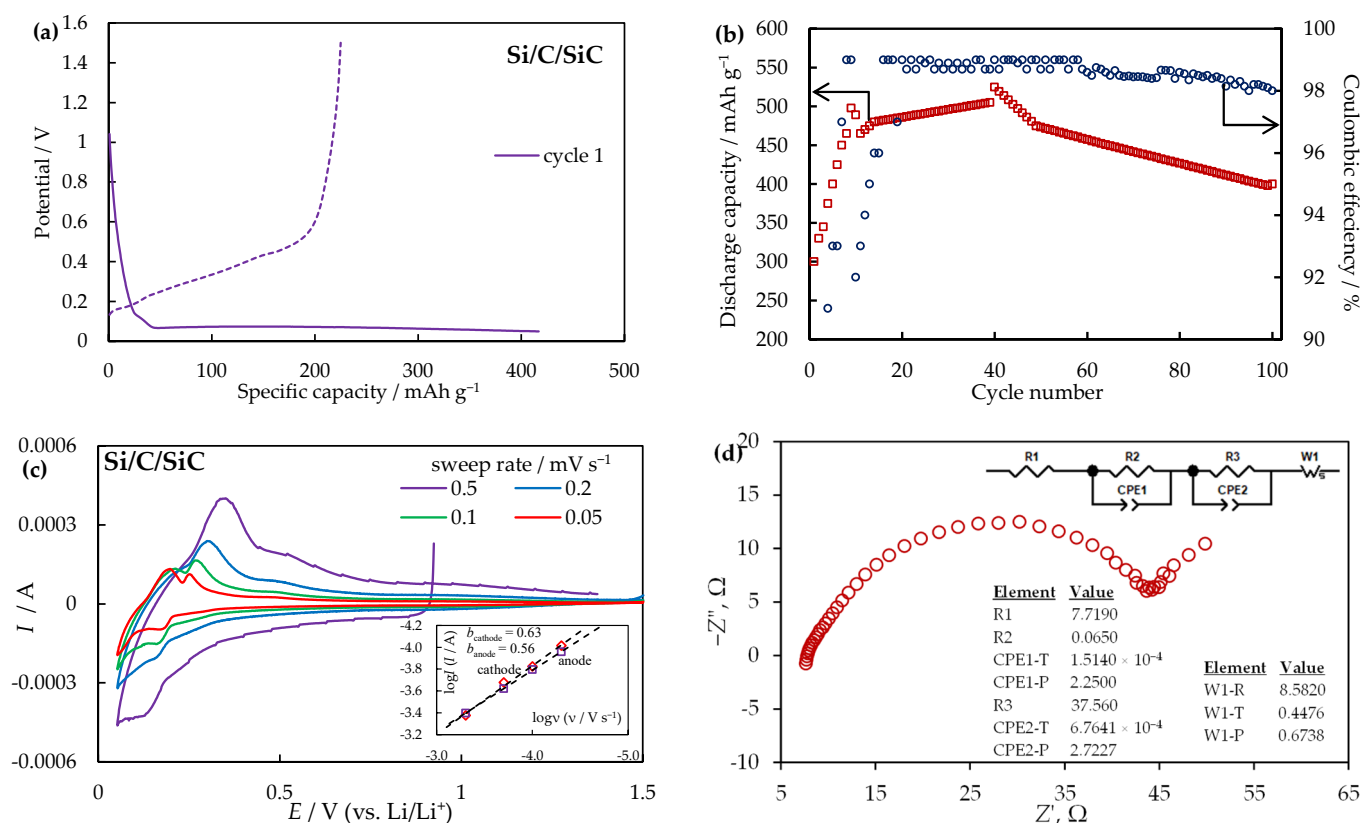


**Figure 9.** Cycling of Si/C/SiC electrode: (a) potential change during first cycle lithiation (dashed line) and delithiation (solid line); (b) discharge capacity and Coulombic efficiency; (c) CVs at different scan rates and log(I)–log(v) dependencies; (d) EIS data with equivalent circuit diagram.

The lithiation mechanism of the Si/C/SiC anode as a whole can be represented by the parallel flow of reactions (2) and (3) as well as reactions (4)–(6):



Accurate estimation of the lithiated products and intermediate products (or its absence) on the basis of peak potentials is difficult. In the literature, there is a very wide spread of the potentials of the occurring reactions and the available analysis methods (EDX, XRD) do not allow one to make a local assessment with the required accuracy when a thick SEI layer is formed.

The partial replacement of SiC with electrodeposited Si leads to an increase in the discharge capacity of the anode, while the cycling stability of the Si/C/SiC composite electrode is lower. In this regard, further work will be aimed at studying the morphology and composition of samples after cycling in order to identify ways to optimize anode composition.

#### 4. Conclusions

Nowadays, one of the most popular issues is connected with the search of anode materials for high energy density lithium-ion batteries. One of the promising materials that meet these requirements are composite materials based on Si/C/SiC mixtures. In such materials, silicon provides increased capacitance, graphite provides high electrical conductivity and SiC provides strength and thermal stability.

In this work, we proposed a new approach for the fabrication of composite anodes based on SiC as well as mixtures of C/SiC and Si/C/SiC. The proposed approach includes carbothermal synthesis and makes it possible to exclude complex equipment and expensive reagents for the anode materials synthesis. Using the proposed method, samples of C/SiC and SiC were synthesized and investigated. A sample of Si/C/SiC was fabricated with the addition of electrodeposited silicon fibers. It was shown that the synthesized SiC is represented by agglomerates of carbide fibers with diameter ranging from 0.1 to 2  $\mu\text{m}$ ; the C/SiC mixture is represented by evenly distributed fibers over the matrix of unreacted graphite; silicon is represented by arbitrary shape fibers with a diameter ranging from 0.45 to 0.55  $\mu\text{m}$ .

Electrochemical behavior of the synthesized samples was studied as part of the anode half-cell of a lithium-ion battery. The possibility of using the obtained samples as part of the composite anode is shown. After 100 cycles pure SiC reached a discharge capacity of 180 and 138  $\text{mAh g}^{-1}$  at a current of C/20 and C, respectively. The mixtures of (wt%) 29.5C-70.5 SiC and 50Si-14.5C-35.5SiC reached a discharge capacity of 328 and 400  $\text{mAh g}^{-1}$  respectively at a C/2 current. The Coulombic efficiency of sample cycling was over 99%. The parameters of the equivalent circuits of the half-cells were estimated and ways to optimize their manufacturing process are noted.

**Author Contributions:** Conceptualization, A.V.S.; methodology, A.M.L., A.S.L. and N.M.L.; validation, A.S.L. and A.V.S.; formal analysis, A.M.L., O.A.B. and N.M.L.; investigation, A.M.L., O.A.B., A.S.L. and N.M.L.; writing—original draft preparation, A.M.L., A.A.T. and A.V.S.; writing—review and editing, A.V.S.; supervision, A.V.S.; project administration, A.V.S. All authors have read and agreed to the published version of the manuscript.

**Funding:** This research received no external funding.

**Institutional Review Board Statement:** Not applicable.

**Informed Consent Statement:** Not applicable.

**Data Availability Statement:** The data presented in this study are available on request from the corresponding author.

**Acknowledgments:** This work is performed in the frame of the State Assignment number 075-03-2022-011 dated 01/14/2022 (the theme number FEUZ-2020-0037). The elemental composition of the samples was analyzed using the equipment of the Central Research Laboratory “Composition of compounds” (IHTE UB RAS).

**Conflicts of Interest:** The authors declare no conflict of interest.

## References

1. Kulova, T.L. New Electrode Materials for Lithium-Ion Batteries (Review). *Russ. J. Electrochem.* **2013**, *49*, 1–25. [[CrossRef](#)]
2. Luo, H.; Wang, Y.; Feng, Y.-H.; Fan, X.-Y.; Han, X.; Wang, P.-F. Lithium-Ion Batteries under Low-Temperature Environment: Challenges and Prospects. *Materials* **2022**, *15*, 8166. [[CrossRef](#)] [[PubMed](#)]
3. Mitsch, T.; Kramer, Y.; Feinauer, J.; Gaiselmann, G.; Markotter, H.; Manke, I.; Hintennach, A.; Schmidt, V. Preparation and Characterization of Li-Ion Graphite Anodes Using Synchrotron Tomography. *Materials* **2014**, *7*, 4455–4472. [[CrossRef](#)]
4. Liu, R.-J.; Yang, L.-X.; Lin, G.-Q.; Bu, H.-P.; Wang, W.-J.; Liu, H.-J.; Zeng, C.-L. Superior electrochemical performances of core-shell structured vanadium oxide@vanadium carbide composites for Li-ion storage. *Appl. Surf. Sci.* **2022**, *588*, 152904. [[CrossRef](#)]
5. Bini, M.; Ambrosetti, M.; Spada, D.  $\text{ZnFe}_2\text{O}_4$ , a Green and High-Capacity Anode Material for Lithium-Ion Batteries: A Review. *Appl. Sci.* **2021**, *11*, 11713. [[CrossRef](#)]
6. Purwanto, A.; Muzayanha, S.U.; Yudha, C.S.; Widiyandari, H.; Jumari, A.; Dyartanti, E.R.; Nizam, M.; Putra, M.I. High Performance of Salt-Modified-LTO Anode in  $\text{LiFePO}_4$  Battery. *Appl. Sci.* **2020**, *10*, 7135. [[CrossRef](#)]
7. Zhang, Y.; Wang, N.; Bai, Z. The Progress of Cobalt-Based Anode Materials for Lithium Ion Batteries and Sodium Ion Batteries. *Appl. Sci.* **2020**, *10*, 3098. [[CrossRef](#)]
8. Feng, Y.; Zhang, H.; Li, W.; Fang, L.; Wang, Y. Targeted Synthesis of Novel Hierarchical Sandwiched NiO/C Arrays as High-Efficiency Lithium Ion Batteries Anode. *J. Power Sources* **2016**, *301*, 78–86. [[CrossRef](#)]
9. Spinner, N.; Mustain, W.E. Nanostructural Effects on the Cycle Life and  $\text{Li}^+$  Diffusion Coefficient of Nickel Oxide Anodes. *J. Electroanal. Chem.* **2013**, *711*, 8–16. [[CrossRef](#)]

10. Gevel, T.; Zhuk, S.; Leonova, N.; Leonova, A.; Trofimov, A.; Suzdaltsev, A.; Zaikov, Y. Electrochemical Synthesis of Nano-Sized Silicon from KCl–K<sub>2</sub>SiF<sub>6</sub> Melts for Powerful Lithium-Ion Batteries. *Appl. Sci.* **2021**, *11*, 10927. [[CrossRef](#)]
11. Feng, K.; Li, M.; Liu, W.; Kashkooli, A.G.; Xiao, X.; Cai, M.; Chen, Z. Silicon-Based Anodes for Lithium-Ion Batteries: From Fundamentals to Practical Applications. *Small* **2018**, *14*, 1702737. [[CrossRef](#)] [[PubMed](#)]
12. Ha, Y.; Schulze, M.C.; Frisco, S.; Trask, S.E.; Teeter, G.; Neale, N.R.; Veith, G.M.; Johnson, C.S. Li<sub>2</sub>O-Based Cathode Additives Enabling Prelithiation of Si Anodes. *Appl. Sci.* **2021**, *11*, 12027. [[CrossRef](#)]
13. Suzdaltsev, A. Silicon Electrodeposition for Microelectronics and Distributed Energy: A Mini-Review. *Electrochem* **2022**, *3*, 760–768. [[CrossRef](#)]
14. Yang, X.; Tachikawa, N.; Katayama, Y.; Li, L.; Yan, J. Effect of the Pillar Size on the Electrochemical Performance of Laser-Induced Silicon Micropillars as Anodes for Lithium-Ion Batteries. *Appl. Sci.* **2019**, *9*, 3623. [[CrossRef](#)]
15. Stokes, K.; Flynn, G.; Geaney, H.; Bree, G.; Ryan, K.M. Axial Si–Ge Heterostructure Nanowires as Lithium-Ion Battery Anodes. *Nano Lett.* **2018**, *18*, 5569–5575. [[CrossRef](#)] [[PubMed](#)]
16. Chockla, A.M.; Klavetter, K.C.; Mullins, C.B.; Korgel, B.A. Solution-Grown Germanium Nanowire Anodes for Lithium-Ion Batteries. *ACS Appl. Mater. Interfaces* **2012**, *4*, 4658–4664. [[CrossRef](#)]
17. Kulova, T.L.; Skundin, A.M. Germanium in Lithium-Ion and Sodium-Ion Batteries (A Review). *Russ. J. Electrochem.* **2022**, *57*, 1105–1137. [[CrossRef](#)]
18. Liu, X.; Zhu, X.; Pan, D. Solutions for the Problems of Silicon–Carbon Anode Materials for Lithium-Ion Batteries. *R. Soc. Open Sci.* **2018**, *5*, 172370. [[CrossRef](#)]
19. Kolosov, D.A.; Glukhova, O.E. Theoretical Study of a New Porous 2D Silicon-Filled Composite Based on Graphene and Single-Walled Carbon Nanotubes for Lithium-Ion Batteries. *Appl. Sci.* **2020**, *10*, 5786. [[CrossRef](#)]
20. Abe, Y.; Saito, I.; Tomioka, M.; Kabir, M.; Kumagai, S. Effects of Excessive Prelithiation on Full-Cell Performance of Li-Ion Batteries with a Hard-Carbon/Nanosized-Si Composite Anode. *Batteries* **2022**, *8*, 210. [[CrossRef](#)]
21. Hou, Y.; Yang, Y.; Meng, W.; Lei, B.; Ren, M.; Yang, X.; Wang, Y.; Zhao, D. Core-Shell Structured Si@Cu Nanoparticles Encapsulated in Carbon Cages as High-Performance Lithium-Ion Battery Anodes. *J. Alloys Compd.* **2021**, *874*, 159988. [[CrossRef](#)]
22. Fan, Z.; Wang, Y.; Zheng, S.; Xu, K.; Wu, J.; Chen, S.; Liang, J.; Shi, A.; Wang, Z. A Submicron Si@C Core-Shell Intertwined with Carbon Nanowires and Graphene Nanosheet as a High-Performance Anode Material for Lithium Ion Battery. *Energy Storage Mater.* **2021**, *39*, 1–10. [[CrossRef](#)]
23. Zhang, X.; Min, B.-I.; Wang, Y.; Hayashida, R.; Tanaka, M.; Watanabe, T. Preparation of Carbon-Coated Silicon Nanoparticles with Different Hydrocarbon Gases in Induction Thermal Plasma. *J. Phys. Chem. C* **2021**, *125*, 15551–15559. [[CrossRef](#)]
24. Liu, G.; Yang, Y.; Lu, X.; Qi, F.; Liang, Y.; Trukhanov, A.; Wu, Y.; Sun, Z.; Lu, X. Fully Active Bimetallic Phosphide Zn<sub>0.5</sub>Ge<sub>0.5</sub>P: A Novel High-Performance Anode for Na-Ion Batteries Coupled with Diglyme-Based Electrolyte. *ACS Appl. Mater. Interfaces* **2022**, *14*, 31803–31813. [[CrossRef](#)] [[PubMed](#)]
25. Liu, G.; Wang, N.; Qi, F.; Lu, X.; Liang, Y.; Sun, Z. Novel Ni–Ge–P Anodes for Lithium-Ion Batteries with Enhanced Reversibility and Reduced Redox Potential. *Inorg. Chem. Front.* **2023**, *in press*. [[CrossRef](#)]
26. Sierra, L.; Gibaja, C.; Torres, I.; Salagre, E.; Avilés Moreno, J.R.; Michel, E.G.; Ocón, P.; Zamora, F. Alpha-Germanium Nanolayers for High-Performance Li-ion Batteries. *Nanomaterials* **2022**, *12*, 3760. [[CrossRef](#)] [[PubMed](#)]
27. Liang, Y.; Chen, Y.; Ke, X.; Zhang, Z.; Wu, W.; Lin, G.; Zhou, Z.; Shi, Z. Coupling of Triporosity and Strong Au–Li Interaction to Enable Dendrite-Free Lithium Plating/Stripping for Long-Life Lithium Metal Anodes. *J. Mater. Chem. A* **2020**, *8*, 18094. [[CrossRef](#)]
28. Sun, X.; Shao, C.; Zhang, F.; Li, Y.; Wu, Q.-H.; Yang, Y. SiC Nanofibers as Long-Life Lithium-Ion Battery Anode Materials. *Front. Chem.* **2018**, *6*, 166. [[CrossRef](#)]
29. Huang, X.D.; Zhang, F.; Gan, X.F.; Huang, Q.A.; Yang, J.Z.; Lai, T.; Tang, W.M. Electrochemical Characteristics of Amorphous Silicon Carbide Film as a Lithium-Ion Battery Anode. *RSC Adv.* **2018**, *8*, 5189–5196. [[CrossRef](#)]
30. Schmidt, H.; Jerliu, B.; Hüger, E.; Stahnc, J. Volume Expansion of Amorphous Silicon Electrodes During Potentiostatic Lithiation of Li-ion Batteries. *Electrochem. Comm.* **2020**, *115*, 106738. [[CrossRef](#)]
31. Liu, G.; Wei, Y.; Li, T.; Gu, Y.; Guo, D.; Wu, N.; Qin, A.; Liu, X. Green and Scalable Fabrication of Sandwich-like NG/SiO<sub>x</sub>/NG Homogenous Hybrids for Superior Lithium-Ion Batteries. *Nanomaterials* **2021**, *11*, 2366. [[CrossRef](#)] [[PubMed](#)]
32. Lou, D.; Chen, S.; Langrud, S.; Razaq, A.A.; Mao, M.; Younes, H.; Xing, W.; Lin, T.; Hong, H. Scalable Fabrication of Si-Graphene Composite as Anode for Li-ion Batteries. *Appl. Sci.* **2022**, *12*, 10926. [[CrossRef](#)]
33. Jo, M.; Sim, S.; Kim, J.; Oh, P. Micron-Sized SiO<sub>x</sub>–Graphite Compound as Anode Materials for Commercializable Lithium-Ion Batteries. *Nanomaterials* **2022**, *12*, 1956. [[CrossRef](#)] [[PubMed](#)]
34. Jumari, A.; Yudha, C.S.; Widiyandari, H.; Lestari, A.P.; Rosada, R.A.; Santosa, S.P.; Purwanto, A. SiO<sub>2</sub>/C Composite as a High Capacity Anode Material of LiNi<sub>0.8</sub>Co<sub>0.15</sub>Al<sub>0.05</sub>O<sub>2</sub> Battery Derived from Coal Combustion Fly Ash. *Appl. Sci.* **2020**, *10*, 8428. [[CrossRef](#)]
35. Galashev, A.; Vorob'ev, A. An Ab Initio Study of Lithization of Two-Dimensional Silicon–Carbon Anode Material for Lithium-Ion Batteries. *Materials* **2021**, *14*, 6649. [[CrossRef](#)] [[PubMed](#)]
36. Shao, Y.; Wang, S.; Li, X. The Effect of Silicon-Containing Minerals on Coal Evolution at High-Temperature Pre-Graphitization Stage. *Minerals* **2023**, *13*, 20. [[CrossRef](#)]
37. Lee, K.-J.; Kang, Y.; Kim, Y.H.; Baek, S.W.; Hwang, H. Synthesis of Silicon Carbide Powders from Methyl-Modified Silica Aerogels. *Appl. Sci.* **2020**, *10*, 6161. [[CrossRef](#)]

38. Xing, Z.; Lu, J.; Ji, X. A Brief Review of Metallothermic Reduction Reactions for Materials Preparation. *Small Methods* **2018**, *2*, 1800062. [[CrossRef](#)]
39. Zhang, Y.; Hu, K.; Zhou, Y.; Xia, Y.; Yu, N.; Wu, G.; Zhu, Y.; Wu, Y.; Huang, H. A Facile, One-Step Synthesis of Silicon/Silicon Carbide/Carbon Nanotube Nanocomposite as a Cycling-Stable Anode for Lithium Ion Batteries. *Nanomaterials* **2019**, *9*, 1624. [[CrossRef](#)]
40. Lebedev, A.S.; Suzdaltsev, A.V.; Anfilogov, V.N.; Farlenkov, A.S.; Porotnikova, N.M.; Vovkotrub, E.G.; Akashev, L.A. Carbothermal Synthesis, Properties, and Structure of Ultrafine SiC Fibers. *Inorg. Mat.* **2020**, *56*, 20–27. [[CrossRef](#)]
41. Anfilogov, V.N.; Lebedev, A.V.; Ryzhkov, V.M.; Blinov, I.A. Carbothermal Synthesis of Nanoparticulate Silicon Carbide in a Self-Contained Protective Atmosphere. *Inorg. Mat.* **2016**, *52*, 655–660. [[CrossRef](#)]
42. Gevel, T.; Zhuk, S.; Suzdaltsev, A.V.; Zaikov, Y.P. Study into the Possibility of Silicon Electrodeposition from a Low-Fluoride KCl–K<sub>2</sub>SiF<sub>6</sub> Melt. *Ionics* **2022**, *28*, 3537–3545. [[CrossRef](#)]
43. Nakashima, S.; Harima, H. Raman Investigation of SiC Polytypes. *Phys. Status Solidi A* **1997**, *162*, 39–64. [[CrossRef](#)]
44. Xing, Z.; Wang, B.; Halsted, J.K.; Subashchandrabose, R.; Stickleb, W.F.; Ji, X. Direct Fabrication of Nanoporous Graphene from Graphene Oxide by Adding a Gasification Agent to a Magnesiothermic Reaction. *Chem. Commun.* **2015**, *51*, 1969. [[CrossRef](#)] [[PubMed](#)]
45. Brodova, I.; Yolshina, L.; Razorenov, S.; Rasposienko, D.; Petrova, A.; Shirinkina, I.; Shorokhov, E.; Muradymov, R.; Garkushin, G.; Savinykh, A. Effect of Grain Size on the Properties of Aluminum Matrix Composites with Graphene. *Metals* **2022**, *12*, 1054. [[CrossRef](#)]
46. Hossain, S.T.; Johra, F.T.; Jung, W.-G. Fabrication of Silicon Carbide from Recycled Silicon Wafer Cutting Sludge and Its Purification. *Appl. Sci.* **2018**, *8*, 1841. [[CrossRef](#)]
47. Martínez-Periñán, E.; Foster, C.W.; Down, M.P.; Zhang, Y.; Ji, X.; Lorenzo, E.; Kononovs, D.; Saprykin, A.I.; Yakovlev, V.N.; Pozdnyakov, G.A.; et al. Graphene Encapsulated Silicon Carbide Nanocomposites for High and Low Power Energy Storage Applications. *J. Carbon Res.* **2017**, *3*, 20. [[CrossRef](#)]
48. Masias, A.; Marcicki, J.; Paxton, W.A. Opportunities and Challenges of Lithium Ion Batteries in Automotive Applications. *ACS Energy Lett.* **2021**, *6*, 621–630. [[CrossRef](#)]
49. Hosen, M.S.; Gopalakrishnan, R.; Kalogiannis, T.; Jaguemont, J.; Van Mierlo, J.; Berecibar, M. Impact of Relaxation Time on Electrochemical Impedance Spectroscopy Characterization of the Most Common Lithium Battery Technologies—Experimental Study and Chemistry-Neutral Modeling. *World Electr. Veh. J.* **2021**, *12*, 77. [[CrossRef](#)]
50. Maddipatla, R.; Loka, C.; Choi, W.J.; Lee, K.-S. Nanocomposite of Si/C Anode Material Prepared by Hybrid Process of High-Energy Mechanical Milling and Carbonization for Li-Ion Secondary Batteries. *Appl. Sci.* **2018**, *8*, 2140. [[CrossRef](#)]
51. Choi, J.-H.; Choi, S.; Cho, J.S.; Kim, H.-K.; Jeong, S.M. Efficient Synthesis of High Areal Capacity Si@Graphite@SiC Composite Anode Material via One-Step Electro-deoxidation. *J. Alloys Compd.* **2022**, *896*, 163010. [[CrossRef](#)]
52. Galashev, A.Y.; Vorob'ev, A.S. First Principle Modeling of a Silicene Anode for Lithium Ion Batteries. *Electrochim. Acta* **2021**, *378*, 138143. [[CrossRef](#)]
53. Uxa, D.; Huger, E.; Dorrer, L.; Schmidt, H. Lithium-Silicon Compounds as Electrode Material for Lithium-Ion batteries. *J. Electrochem. Soc.* **2020**, *167*, 130522. [[CrossRef](#)]
54. Jiang, Y.; Offer, G.; Jiang, J.; Marinescu, M.; Wang, H. Voltage Hysteresis Model for Silicon Electrodes for Lithium Ion Batteries, Including Multi-Step Phase Transformations, Crystallization and Amorphization. *J. Electrochem. Soc.* **2020**, *167*, 130533. [[CrossRef](#)]

**Disclaimer/Publisher's Note:** The statements, opinions and data contained in all publications are solely those of the individual author(s) and contributor(s) and not of MDPI and/or the editor(s). MDPI and/or the editor(s) disclaim responsibility for any injury to people or property resulting from any ideas, methods, instructions or products referred to in the content.